Chapter 4:

Microstructural and light emission properties of $ZnSnP_2$ thin film absorber: study of native defects

4.1. Introduction

Since the last few decades the main goal of the material science research to find a replacement of silicon (Si) for the fabrication of optoelectronic devices which will be used in our day to day uses. A ternary compound semiconductor, $ZnSnP_2$, belonging to the group II-IV-V_2 has the potential to become a good replacement of Si, considering the fact that it is a direct bandgap semiconductor and all the constituent elements are eco-friendly and earth-abundant. For large scale device production, the successful deposition of thin-film and the detailed understanding of its light emission/absorption properties are essential.

The fabrication of good quality (uniform thickness, minimal surface roughness, etc.) and a stoichiometric thin film is necessary for future device applications. Section 2.3.2. of chapter 1 describes different processes that have already been implemented for the deposition of $ZnSnP_2$ thin film, by other researchers till now. However, most of those techniques are expensive and complicated, thus they are not suitable for the large scale production of the $ZnSnP_2$ epitaxial layer. In view of these, fabrication of good quality $ZnSnP_2$ thin film by inexpensive and simple processes is essential

The first successful growth of $ZnSnP_2$ in bulk form was done by Valpolin et. al. long-time ago [1]. However, despite its interesting optical and electronic properties, still, the application of $ZnSnP_2$ in the optoelectronic devices has not been done extensively. Recently, $ZnSnP_2$ based thin-film solar cell with $ZnSnP_2$ absorber is fabricated by the phosphidation method under the variation of the Zn/Sn atomic ratio [2]. The solar cell parameters (J_{SC} = 2.63 mA/cm^2, V_{OC} - =3.7 mV, FF = 27.2%, and conversion efficiency = 0.0027%) have been measured using near-stoichiometric $ZnSnP_2$ as the absorber layer. In the study, the authors found two different current areas. The low-current area is attributed to the presence of the Zn_3P_2 secondary phase forming the shunt paths while the high-current area (0.014 cm^2) with efficiency = 0.021%, J_{SC} = 5.03 mA/cm^2 is obtained due the formation of pure $ZnSnP_2$ phase. The energy band gap of $ZnSnP_2$ thin film prepared by the phosphidation method was reported as 1.38 eV indicating the growth of partially ordered $ZnSnP_2$ structure with an appropriate variation of Zn/Sn atomic ratio. Nakatsuka et al [3, 4] studied the J–V characteristics of the heterojunction solar cell [Al/AZO/ ZnO/CdS/$ZnSnP_2$/Mo]. The performance of the fabricated cell was found quite low (conversion efficiency is 0.087%). Necessary modifications of the cell structure to achieve better performances such as improvement of the resistance of the hetero-interfaces and the use of appropriate buffer materials have been suggested.

Though some limited studies have been made by several researchers on the preparation of crystalline bulk material and thin epitaxial layer, detailed understanding of the optical and electrical properties, the nature of native defects responsible to p-type conductivity in $ZnSnP_2$ are still obscure. Defects introduce localized levels in the energy gap of semiconductors through which often become the deciding factor of the device performance, efficiency, and reliability [5]. Native defects such as vacancies, self-interstitials, and antisite defects often act as unintended dopants or compensate intentionally introduced dopants [6]. In addition, native defects, as well as contaminant impurities, introduce deep level traps limit the efficiency of optoelectronic devices [7], cause degradation of power devices [5]. Thus, with the ultimate aim of device fabrication, it is of great significance to study the nature, behavior, and position of such defects under different conditions. It is well established that the temperature and excitation power-dependent PL measurement is an extremely reliable technique for the identification of defects.

This chapter of the thesis contains the thin films deposition of $ZnSnP_2$ on p-type silicon (001), sapphire and glass substrate by PVD technique at an elevated temperature. The basic characterizations such as XRD, SEM, HRTEM, reflectance and transmittance spectroscopy and PL measurement at a low temperature of the as-deposited thin films were performed. The emission characteristics and their close relation to the intrinsic defects in the $ZnSnP_2$ films are discussed.

4.2. Experimental

4.2.1. Bulk $ZnSnP_2$ growth

The bulk growth of $ZnSnP_2$ was carried out by the direct chemical reaction of the constituent elements (Zn, Sn, and P). Raw materials of Zinc granules (99.9999% Sigma Aldhrich), tin granules (99% Merck) and red Phosphorus nano-powder (99.999% Sigma Aldhrich) were sealed in a quartz ampoule of an inner diameter of 11.6 mm and outer diameter 13.6 mm. Prior to sealing, the quartz tube, Zn & Sn granules were cleaned with the inorganic and organic solvent to remove the unintentional oxide layer and other chemical impurities. 0.1 M HCl and chromic acid were used as the inorganic solvent for cleaning Zn & Sn and quartz tube, respectively. Thereafter, Zn, Sn granules and quartz tube were washed using deionized water. Finally, all of them were cleaned with acetone and dried. Before the sealing, the ampoule was taken away to a vacuum of 10^{-3} mbar. At the time of sealing extra effort was given to prevent

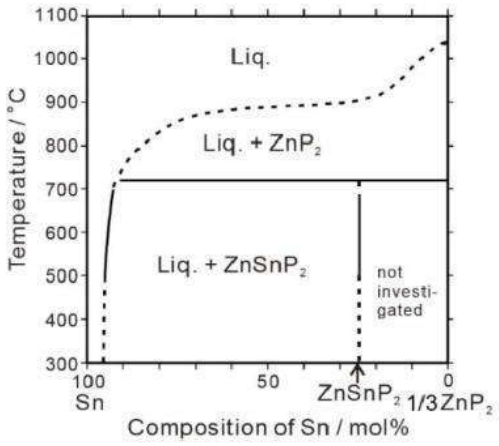

Figure 4.1. Pseudo-binary phase diagram of the ZnP_2-Sn system [3].

the temperature increase in the portion of the ampoule that contains the reactants. It is very important owing to the relatively low melting point (232 ºC) of Sn. For the preparation of $ZnSnP_2$ bulk crystal, the pseudo-binary phase diagram of the Sn-ZnP_2 system (Figure 4.1) was considered and the ampoule sealing was accomplished under excess Sn (with 89.9 mole% Sn concentration) condition to counteract the excess vapor pressure of phosphorus. [8, 9]. Thereafter, the quartz ampoule was properly placed at the constant heating region inside a custom-designed vertical single zone tube furnace. The temperature of the furnace was stepped up to 500º C with a constant ramp rate of 4º C per minute. Then it was kept fixed at 500º C for two hours. Thereafter, the temperature of the furnace was once again increased to 600º C with a fixed ramp rate of 5º C per minute and kept fixed for one hour. Finally, the temperature is further moved up to 700º C with a uniform ramp rate of 5º C per minute and kept constant for 24 hours. Finally, the ampoule was rapidly cooled to room temperature. Bulk crystal obtained after this process was treated by 0.1M HCl to remove the excess Sn and the dark greyish precipitate was collected in the form of powder.

4.2.2. Deposition of $ZnSnP_2$ thin film

The obtained $ZnSnP_2$ powder as discussed in section 4.2.1 was utilized as the source material to deposit the thin film, on p-Si, sapphire and glass substrate by e-beam evaporation. The evaporent was kept inside the boat-shaped molybdenum crucible. the substrates were chemically cleaned to remove any surface impurities before placing them into the growth chamber. Si and sapphire were treated with hydrofluoric acid whereas the glass was cleaned with chromic acid. Subsequently, all three substrates were washed with acetone and dried.

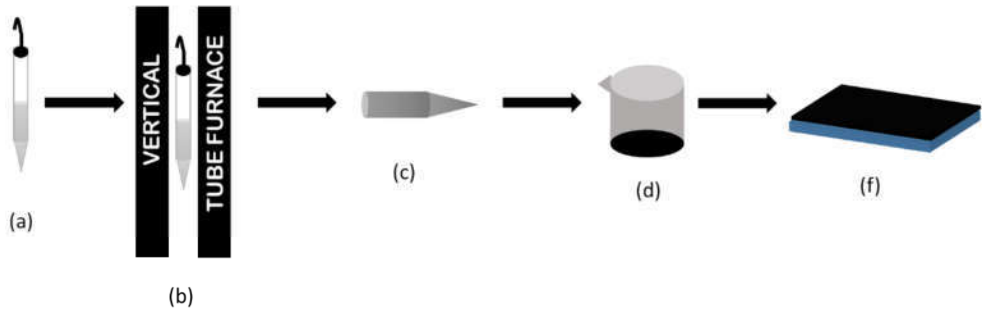

Figure 4.2. Schematic representation of the growth process. (a) ampoule containing Zn, Sn and P was sealed (b) Placed in a vertical tube furnace and heated 700 °C for 24 hours (c) Ingot was obtained (d) Ingot was treated with 0.1 MHCl to remove Sn (d) Thin-film was deposited by e-beam evaporation.

Throughout the deposition time, the substrates were maintained at a constant temperature of 250 °C. The Growth rate and the film thickness measured by the quartz crystal monitor were about 0.10 nm/s and 43 nm, respectively. The constant deposition rate was achieved by maintaining a fixed electron beam current of 40 mA. During the entire procedures, the air pressure within the growth chamber was approximately 10^{-6} mbar. The execution of all the processes was carried out in the instrument named as smart coat 3.0 manufactured by Hind High Vacuum. A schematic representation of the growth process is shown in Figure 4.2.

4.2.3. Characterization

4.2.3.1. Structural and morphological study

The as-grown $ZnSnP_2$ powder and thin film were examined by the XRD, GIXRD and XRR technique respectively using Rigaku Smart Lab. The surface morphology of the films was investigated using FESEM (Quanta 200 FEG). High-resolution transmission electron microscopy (HRTEM, Tecnai G^2 F30 S-TWIN) was used to study the microstructure and crystallinity of the films deposited on Si (001) substrate in cross-sectional mode.

4.2.3.2. Optical characterization

The reflectance (R) and transmittance (T) measurements of the deposited thin film grown on glass substrate were performed with the help of the Perkin-Elmer lambda-750 spectrophotometer equipped with 150 mm integrating sphere assembly. Efforts have been given to eliminate the contribution of the substrate in the reflectance and transmittance measurements of $ZnSnP_2$ thin films. For the reflectance measurement, a black paper has been inserted behind the transparent glass and sapphire substrates to prevent reflectance from the

substrate-air interface. On the other hand, the transmittance of the film-substrate structure has been obtained by eliminating the absorption due to pure substrate by placing a substrate in the reference beam. Film grown on the sapphire substrate was used to record the PL spectra in the temperature ranging from 15 K – 200 K. The PL measurement was carried out using 488 nm Ar-Ne excitation laser sources. Furthermore, we have employed the hot probe method for identifying the nature of the conductivity of the sample.

4.3 Result and discussion

4.3.1. XRD study of the bulk $ZnSnP_2$

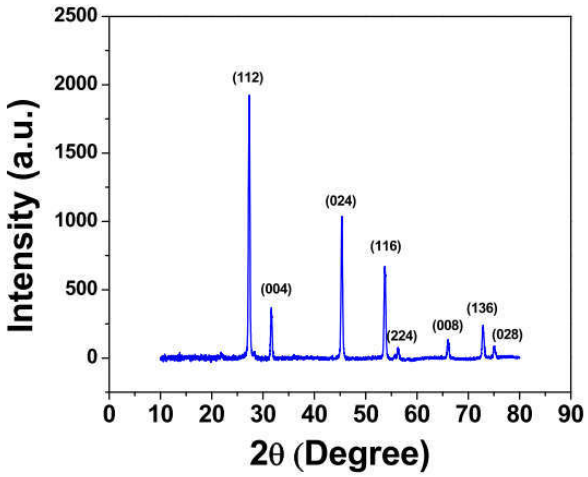

Figure 4.3. X-ray diffraction pattern of the bulk $ZnSnP_2$.

Before considering the $ZnSnP_2$ powder as the source material in the e-beam evaporation process for thin film deposition, the routine XRD technique was employed to have an idea about its structure. The result is represented in Figure 4.3. All diffraction peaks corresponding to (112), (004), (024), (116), (224), (008), (136) and (028) planes of the chalcopyrite structure of $ZnSnP_2$ are identified by comparing the available JCPDS data of $ZnSnP_2$ [JCPDS File: 73-0396]. It thus signifies that we have successfully synthesized the chalcopyrite $ZnSnP_2$ in powder form.

4.3.2. GIXRD study of the $ZnSnP_2$ thin film

Considering the thickness of 43 nm as obtained from the quartz crystal monitor data, the GIXRD technique was employed for evaluating the structural information which is depicted in Figure 4.4. The as-deposited thin film exhibit peaks at $2\Theta = 44.50^0$ and 63.45^0 corresponding to the diffraction planes (024) and (008) of chalcopyrite $ZnSnP_2$ structure.

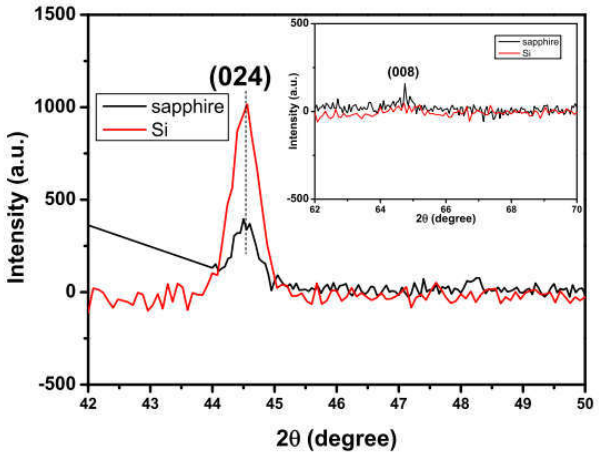

Figure 4.4. GIXRD data of the thin film.

4.3.3. XRR of the $ZnSnP_2$ thin film

Figure. 4.5 (a) shows XRR of the grown film. In the Distorted Wave Born Approximation (DWBA) formalism (details is given in Appendix I) the total thickness of the films was divided into 100 elemental boxes and the size of each box is chosen as 5 Å. While choosing the box size, it is worthwhile to note that the box size must be smaller than the minimum features within

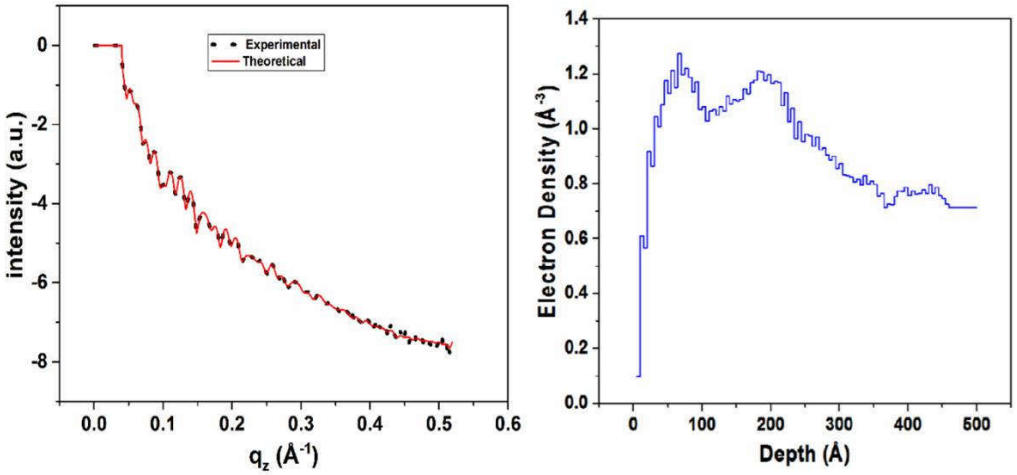

Figure.4.5. (a) Experimentally obtained XRR curve for the thin film and as well as the theoretically generated data using DWBA formalism. (b) The obtained EDP.

the grown structure. Initial guess value is provided for each box counting to 100 numbers of guesses. The Levenberg-Marquardt algorithm was used for the nonlinear least-square fitting program to fit the experimental data on the basis of DWBA formalism. We were unable to fit the experimental data considering a single layer of $ZnSnP_2$ alone. The structure was then

assumed as a bilayer of $ZnSnP_2$ and native SiO_2 on Si substrate. Figure. 4.5(a) shows the fitted data almost replicates the experimentally obtained data. The corresponding electron density profile (EDP) with the depth of the grown structure is shown in Figure. 4.5 (b).

Electron density (ED) of the top surface agrees quite well with that of the $ZnSnP_2$ i.e. 1.2088 $Å^{-3}$. The ED value gradually decreases to 0.8059 $Å^{-3}$ which corresponds to that of the SiO_2 layer. The gradual decrease in the ED value from 1.2088 $Å^{-3}$ to 0.8059 $Å^{-3}$ signifies inter-diffusion between the two layers. Figure. 4.5 (b) shows that after 450Å thickness, the value of ED matches with that of the Si. Interfacial roughness was also used as a parameter in the fitting process. We have obtained 2.5 Å of interface roughness for air-film and 1.2 Å for that of the film-substrate interface.

4.3.4. Microscopy study

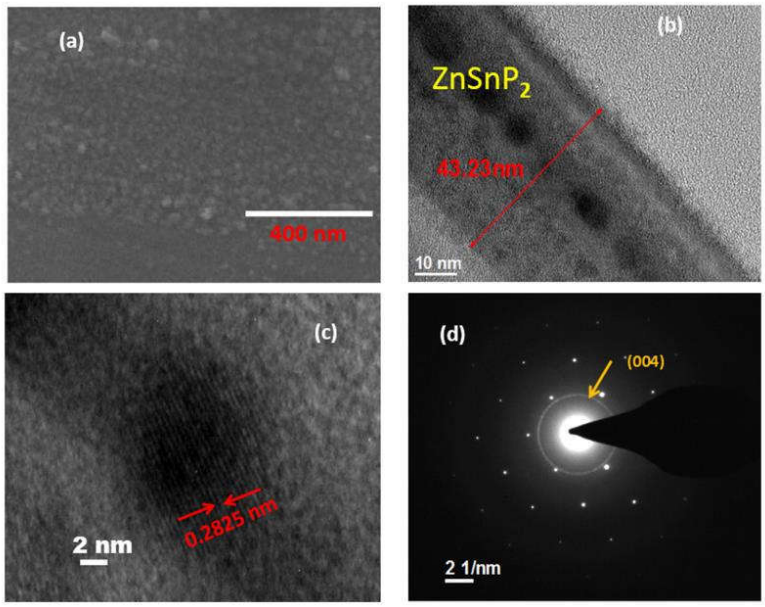

Figure 4.6. (a) Scanning Electron Micrograph of $ZnSnP_2$ thin film. (b) The cross-sectional view of the Transmission Electron Micrograph and (c) Lattice image of $ZnSnP_2$ thin film deposited on silicon (100). (d) Selected area diffraction pattern.

The SEM image of the film is shown in Figure.4.6(a). The surface morphology is uniform and the average grain size is found to be nearly 20 nm. Figure. 4.6(b) shows the HRTEM image of the film, operated in cross-sectional mode. It is clearly observed that the film is not of uniform composition throughout the entire area. A series of dark spots arranged in a line is seen, which is little off-centered towards the surface of the film. A magnified view of one of these spots, shown in Figure. 4.6(c), indicates the growth of nearly uniform crystallites of dimension 10 nm

X 20 nm. An inter-planar spacing of 0.2825 nm corresponding to the (004) plane of $ZnSnP_2$ was obtained from the high-resolution image. In addition to the large crystallites arranged in the line, we also observed relatively smaller crystallites scattered across the film. The SAED pattern has shown in Figure. 4.6(d) which depicts a ring with spotty features superimposed on it. The ring pattern appears because of the random orientation of the lattice planes of one crystallite with respect to another and also due to the contribution from the smaller crystallites. The non-uniform distribution of intensity of the ring is due to the strong spotty pattern from

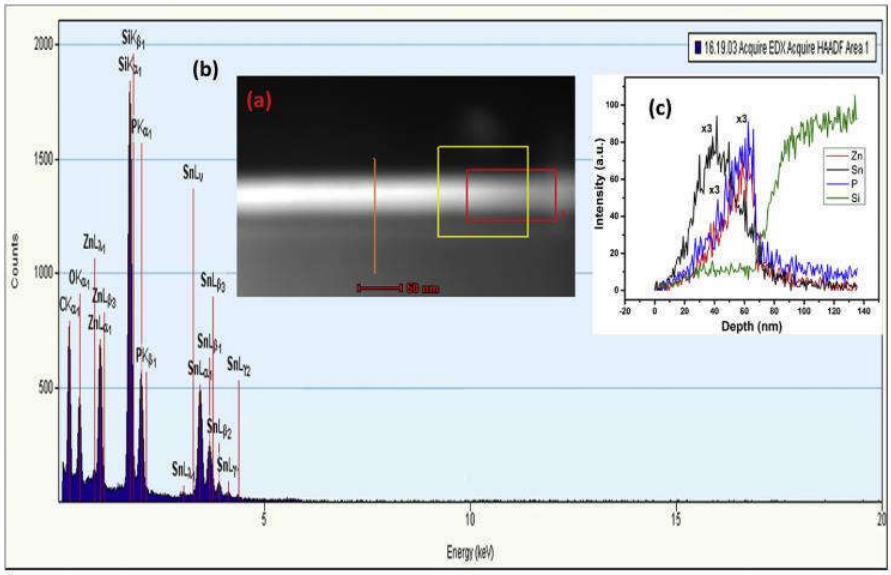

Figure. 4.7. TEM high annular dark field image (cross-sectional view), (b) EDX spectra and (c) depth profile of $ZnSnP_2$ thin film on Si (100) substrate.

the larger crystallites. The inter-planar spacing calculated from the diameter of the ring of the SAED pattern (0.2850 nm) matches closely with that obtained from the high-resolution image (Figure 4.6(c)). To understand the preferential alignment of the bigger crystallites along the line, we have further considered a detailed elemental distribution study implementing EDX analysis (Figure. 4.7) in the HRTEM across the film. Figure. 4.7(a) shows the HADF of the cross-section of the film. Figure 4.7(b) shows the EDX spectra across the region marked by the yellow rectangle of Figure. 4.7(a), which clearly shows peaks due to Zn, Sn and P. The average stoichiometry ratio of Zn:Sn:P, calculated from the integrated intensities and taking care of the sensitivity factors, was found to be within the desired range of 1:1:2 to the accuracy of ~± 10 % as is the case for determination of composition from EDX analysis. The elemental mapping along a line shown by the orange line in Figure. 4.7(a) is shown in the plot of Figure. 4.7(c). Along with the traces for Zn, Sn, and P, the figure also shows elemental distribution

corresponding to Si which is the substrate. The traces corresponding to Zn and P gradually increases till the interface of the film with the substrate, while that of Sn shows a peak at a distance of about ~20 nm from the edge of the film, which is approximately the location of the line of the bigger crystallites of $ZnSnP_2$. The other area of the film is probably consisted of amorphous compounds of Zn and P as well as small crystallites of $ZnSnP_2$. The gradual increase in intensities corresponding to the elements is limited to the detector. All the intensities decreased rather abruptly towards the interface of the film and the substrate. The larger crystallites probably grew at the expense of the smaller ones during the film deposition following the mechanism of Oswald ripening. The arrangement of the ripened crystallites occurred in a line due to a fixed thickness of the film.

4.3.5. Reflectance and transmittance spectra

Figures. 4.8(a) and 4.9(a) represent the typical diffuse reflectance (R) and transmittance (T) spectra of the $ZnSnP_2$ thin films on glass and sapphire substrates respectively in the wavelength interval of 300-2000 nm. The R and T data have been utilized to accurately evaluate the coefficient of absorption coefficient (α) using equation 3.11 of chapter 3. Figure. 4.8(b) depicted the variation of the absorption coefficient of e-beam deposited $ZnSnP_2$ thin films with

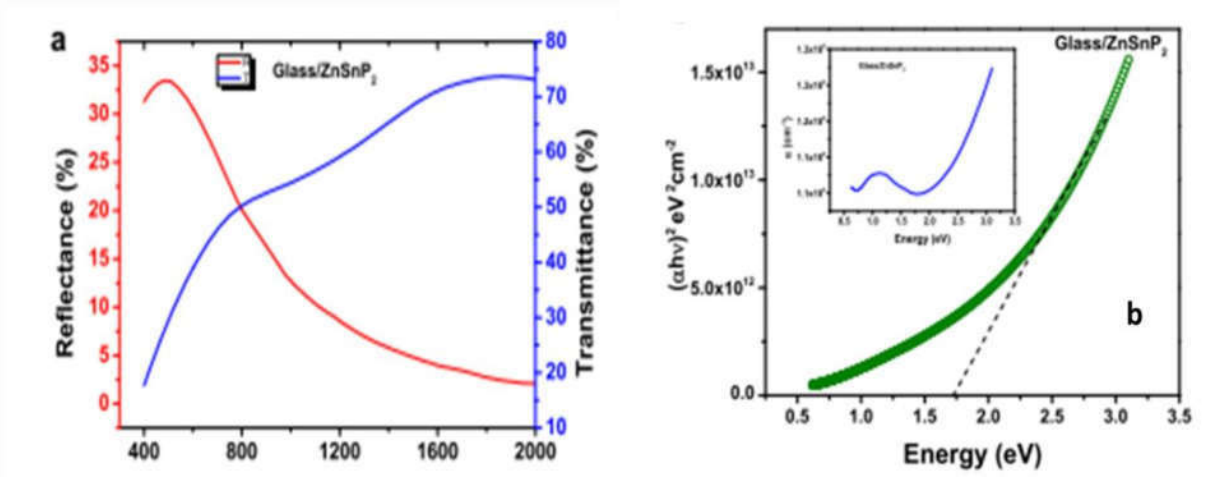

Figure. 4.8 (a). Transmittance and reflectance spectra of $ZnSnP_2$ thin film on the glass substrate. (b). $(\alpha h\nu)^2$ versus hν plot for the calculation of bandgap and optical absorption spectra (inset) of $ZnSnP_2$ thin film on the glass substrate.

photon energy varying from 0.5 eV to 3.0 eV. The optical bandgap of the film has been calculated by plotting $(\alpha h\nu)^2$versus the energy (hν) in eV and extrapolating the linear part of the spectrum, $(\alpha h\nu)^2 = f(h\nu)$, to horizontal axis. A direct bandgap of 1.71 eV of the $ZnSnP_2$

thin film (43 nm thickness) deposited at 250 °C is estimated, which is similar to the recent theoretical calculation (~ 1.71 eV) using modified Becke-Johnson (mBJ) potential [10]. A similar value of bandgap has been estimated for the $ZnSnP_2$ films grown on sapphire substrates as exhibited in Figure. 4.8(b). This result also agrees quite well with the other theoretically predicted value (1.68 eV) for the ordered chalcopyrite $ZnSnP_2$ structure and previously determined experimental value [11]. However, both the $ZnSnP_2$ films exhibit excess optical absorption and considerable band tailing in the low energy region of the spectrum. It should be noted that on the low energy side of the absorption edge in the case of thin films, the excess absorption usually causing an exponential tail that occurs between the various energy states developed near the band edges due to the presence of impurity and defects. The variation of absorption coefficient with photon energy in this low energy region often follows Urbach's rule [12] and usually disturb the band edge related transition.

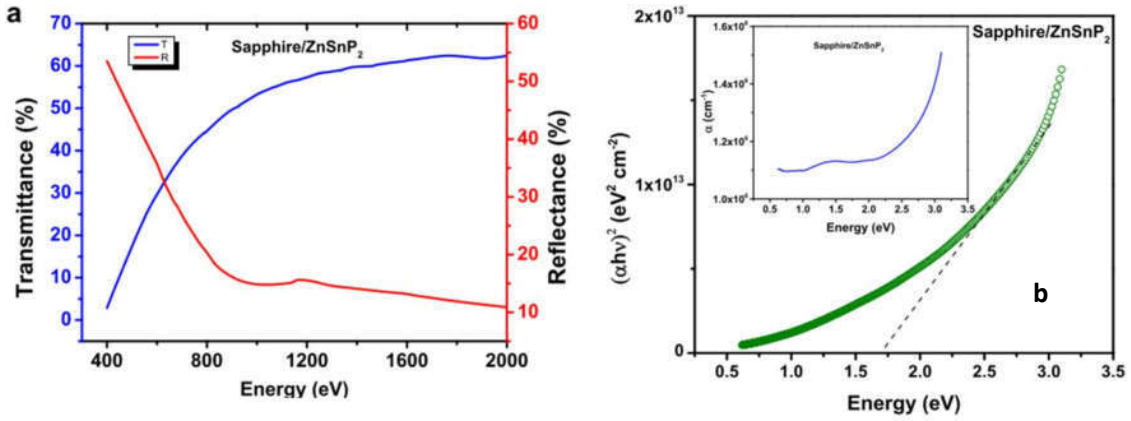

Figure 4.9(a). Transmittance and reflectance spectra of $ZnSnP_2$ thin film on glass substrate. (b). $(\alpha hv)^2$ versus hv plot for the calculation of bandgap and optical absorption spectra (inset) of $ZnSnP_2$ thin film on the sapphire substrate.

4.3.6. Photoluminescence spectra

The temperature (15 – 200 K) and excitation power (13.66 - 77.9 mW) dependent PL measurements were performed to study the origin of the recombination process in $ZnSnP_2$ films grown on sapphire substrates at 250 °C. Temperature-dependent PL spectra are shown in Figure.4.10(a). The overall PL spectra of the sample are non-symmetrical and consist of two broad and overlapped peaks. The first peak appeared at 1.529 eV at 15 K which is red shifted and decreased in intensity with an increase in temperature. The other peak (1.643 eV, at 15 K) which is much broader compared to the first peak also shows similar behavior (Figure. 4.10(b)).

However, the second peak began to quench as the temperature raised above 100 K. Considering the nature of the emission band of the peaks, integrated PL intensity has been plotted in each

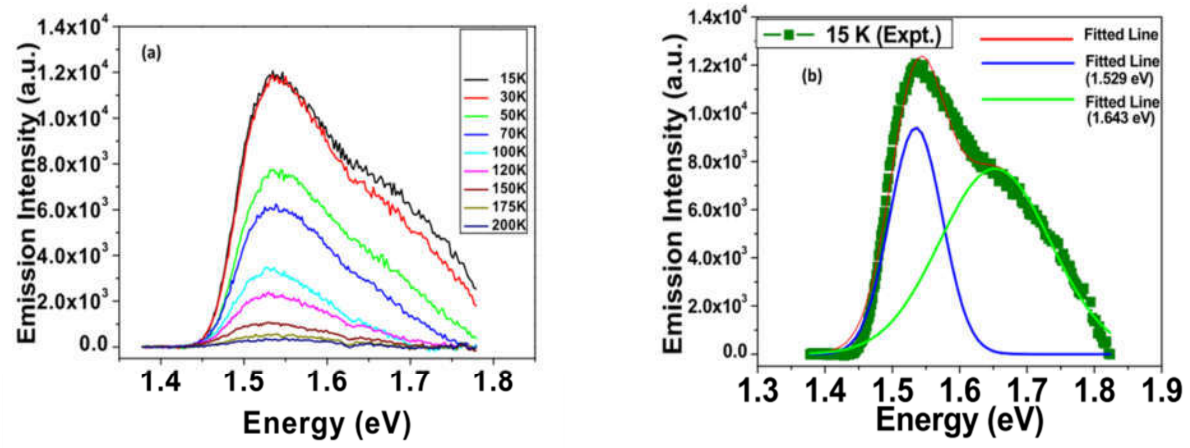

Figure 4.10 (a). Temperature variation of photoluminescence (PL) spectra of $ZnSnP_2$ thin film. (b). De-convoluted PL spectrum recorded at 15 K.

case with inverse temperature in Figure.4.11 and fitted with the two-channel Arrhenius equation [13]:

$$I = \frac{I_0}{1+A\,exp\left(\frac{-E_{T1}}{KT}\right)+B\,exp\left(\frac{-E_{T2}}{KT}\right)} \tag{3.2}$$

where A and B are different process rate parameters, E_{T1} and E_{T2} are two different activation energies at low and high-temperature regions respectively. Fitted parameters are (E_{T1}= 10 meV and E_{T2}= 56 meV) and E_{T1}= 8 meV and E_{T2}= 30 meV) for first and second peaks, respectively, indicating the presence of two thermally activated recombination centers in each case. As the

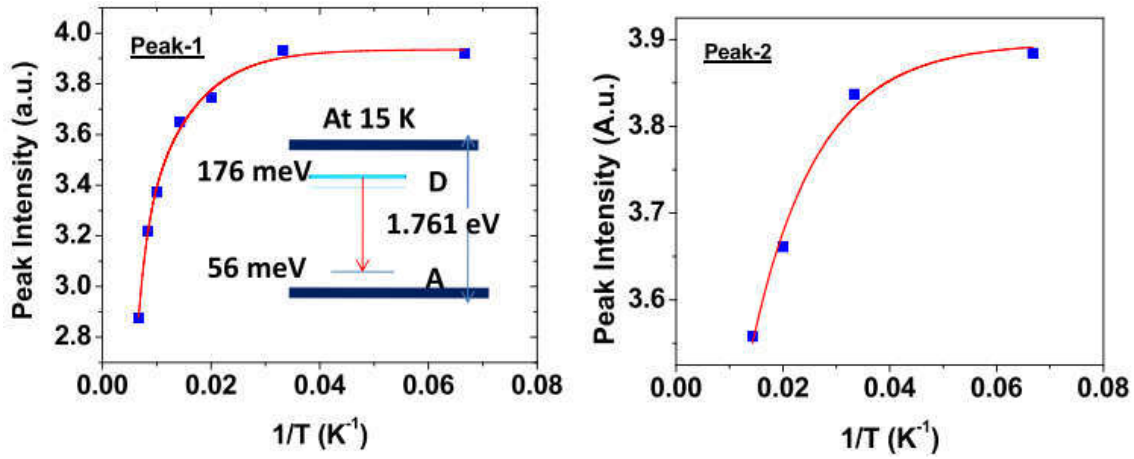

Figure. 4.11. The intensity of peak-1 and peak-2 as a function of reciprocal temperature. Continuous lines are fitted curves using two-channel Arrhenius's equation.

transmittance and reflectance measurements provide the optical band gap, E_g = 1.71 eV at room temperature, the emission bands centered around 1.529 eV cannot be considered as the band to band transition in $ZnSnP_2$. The variation of the emission peak energy, $E_{max}(T)$, with temperature (T), has been also attempted to fit using the Varshni model as follows

$$E_{max}(T) = E\ (0) - \frac{\alpha T^2}{\beta + T}, \tag{3.3}$$

The fitting procedure yielded the values of fitting parameters for the first peak, E (0) = 1.531 eV, ($\alpha = 1.92\ X10^{-4}$ eV/K, $\beta = 56.10$ K), but completely disagreed with the band-edge related transition. However, an idea regarding the variation of bandgap with temperature is obtained. Therefore, it is concluded that the transitions are related to the donor-acceptor pair (DAP) transition due to the presence of native defects in the $ZnSnP_2$ films. The experimental studies [8] and first-principles study of point defects in $ZnSnP_2$ [14] show that the most likely donors are Sn-on-Zn sites [Sn_{Zn}] and acceptors are Zn-on-Sn sites [Zn_{Sn}] and Zn vacancies [V_{Zn}]. The DAP recombination process can be explained using the following relation [15, 16] with the emission peak maxima, E_{max}, as

$$E_{max} = E_g - (E_D + E_A) + \frac{e^2}{4\pi\varepsilon_0\varepsilon R_{DA}}, \tag{3.4}$$

where, E_D and E_A are donor and acceptor activation energies, respectively with their separation (R_{DA}), E_g is the energy band gap and ε is the dielectric constant of $ZnSnP_2$ material. Since the

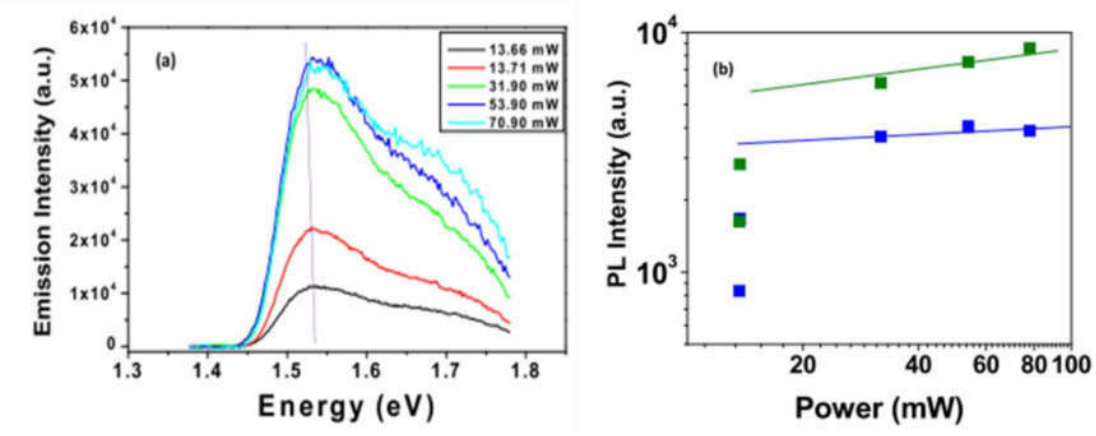

Figure. 4.12. (a). The intensity variation of PL emission with excitation power. (b). The intensity of peak-1 and peak-2 as a function of excitation power

PL data are not available at room temperature, the recombination processes have analyzed at 15 K, using the value of bandgap, E_g (15 K) = 1.761 eV, which has been approximately

determined from the Varshni model. We presumably considered that the donor and acceptor levels are due to [Sn_{Zn}] and [V_{Zn}], respectively and R_{DA} is very large compared to the unit cell dimension and Zn-Sn bond length (~ 0.401 nm). A value of (E_D+E_A) = 232 meV is obtained. Thus, a deep donor level, E_D = (232 - E_{T1}= 232-56) meV = 176 meV from the conduction band (CB) is determined with an acceptor level, E_A = E_{T2} = 56 meV from the valence band (VB). A schematic band model is given as inset in Figure.4.11 for clarifying the radiative recombination process for the first peak. Miyauchi et al [8] explained their PL emission band at about 1.54 eV considering DA pair transition due to similar defects for the bulk $ZnSnP_2$ crystals grown by solution growth and normal freezing methods. However, in our model, the bandgap energy has been considered to correlate to assign the actual donor or acceptor levels.

To explain the origin of the second PL emission peak appeared at 1.643 eV at 15 K, donors at [Sn_{Zn}] sites (E_D=176 meV) and acceptors at [Zn_{Sn}] sites (E_D = E_{T2}= 30 meV) are considered. A calculation similar to the above provides DA pair separation, i.e., $R_{DA}\approx$ 4.4 nm. The value of R_{DA} is roughly 11 times the Sn-Zn bond length [17] and 4 times the unit cell dimension (a=0.5651 nm and c=1.1302 nm) of the $ZnSnP_2$ cell [18], indicating that both the PL peaks are originated from the DA pair transition although their separations are different. In the above calculation, we have used the dielectric constant ($\varepsilon = 8.2$) value for chalcopyrite $ZnSnP_2$ [19]. It is noteworthy to mention that the activation energy (E_{T1}=8-10 meV) at the low-temperature region (Figure. 4.11) is related to the escaping of charge carriers from the band tail states. Our absorption spectrum (Figures. 4.8-4.9) shows considerable band tailing at the low energy region (< 1.4 eV).

We have also investigated the variation of the integrated intensity of PL emission bands with excitation power at 15K (exhibited in Figure. 4.12(a)). It is observed that the PL emission intensity increases with excitation power up to 31 mW and then saturates at the high values of laser power. On the other hand, the PL peaks do not exhibit any appreciable peak shifts with excitation power. A very small blue shift of ~ 4 meV is observed between the emission peaks measured at 13.66 and 70.90 mW, respectively. These observations are indicative of the donor (D)-acceptor (A) pair related recombination process of distant pairs [20]. Figure. 4.12(b) shows the typical variation of PL intensity for both the PL emission bands with laser power. The nature of variation indicates that two emission peaks of different origins have similar in quenching character.

4.4 Conclusion

The successful growth of polycrystalline $ZnSnP_2$ thin films on p-type Si (001), sapphire and glass substrates by e-beam evaporation technique is reported. The selected area electron diffraction pattern justifies the polycrystalline nature of the grown structure ($Si/ZnSnP_2$). The estimation of bandgap from the measured optical reflectance and transmittance spectra at room temperature is found to be 1.71eV. The absorption coefficient of the film is about $> 10^6$ cm^{-1} above 1.6 eV of photon energy. In low-temperature PL measurement, two broad emission peaks have been observed at 1.529 eV and 1.643 eV respectively. DA pair recombination model is considered to explain the luminescence spectra of the $ZnSnP_2$ films. Antisite defects (Sn_{Zn}-acceptor, Zn_{Sn}-donor) and vacancies (V_{Zn}) present in the $ZnSnP_2$ are suggested as native defects and mainly responsible for the light emission property.

References

[1] A. A. Vaipolin, N. A. Goryunova, L. I. Kleshchinskii, G. V. Loshakova andE. O. Osmanov, Phys. Stat. Sol. (1968), 29, 485.

[2] N. Yuzawa, J. Chantana, S. Nakatsuka, Y. Nose and T. Minemoto, Current Appl. Phys. (2017), 17, 557.

[3] S. Nakatsuka, N. Yuzawa, J. Chantana, T. Minemoto and Y. Nose, Phys. Stat. Sol. A, (2016), 1.

[4] S. Nakatsuka, Y. Nose and Y. Shirai, J. Appl. Phys., (2016), 119, 193107.

[5] S. T. Pantelides, Y. Puzyrev, X. Shen, T. Roy, S. Das Gupta, B. R. Tuttle, D. M. Fleetwood, and R. D. Schrimpf, Microelectron. Eng., (2012), 90, 3.

[6] A. García and J. E. Northrup, Phys. Rev. Lett., (1995), 74, 1131.

[7] A. Alkauskas, Q. Yan, and C. G. Van deWalle, Phys. Rev. B, (2014), 90, 075202.

[8] K. Miyauchi, T. Minemura, K. Nakatani, H. Nakanishi, M. Sugiyama, S. Shirakata, Phys. Stat. Sol. C, (2009), 6, 1116.

[9] K. Nakatani, T. Minemura, K. Miyauchi, K. Fukabori, H. Nakanishi, M. Sugiyama and S. Shirakata, Jpn. J. Appl. Phys., (2008), 47, 5342.

[10] R.A. Smith, Semiconductors, Cambridge University Press, Cambridge (1986).

[11] P. St-Jean, G.A. Seryogin and S. Francoer, Appl. Phys. Lett., (2009), 96, 231913.

[12] F. Tran and P. Blaha, Phys. Rev. Lett., (2009), 102, 226401.

[13] W. Stadler, D.M. Hofmann, H.C. Alt, T. Muschik and B.K. Meyer, Phys. Rev. B, (1995), 51, 10619.

[14] S. Ebraheem and A. El-Saied, Mater. Sci. Application., (2013), 4, 324.

[15] A. Nayak and D.R. Rao, Appl. Phys. Lett., (1993), 63, 592.

[16] R.C.C. Lite and A.E. Digiovani, Phys. Rev., (1963), 153, 841.

[17] Yu Kumagai, M. Choi, Y. Nose and F. Oba, Phys. Rev. B, (2014), 90, 125202.

[18] A. Nayak and D. R. Rao, Optical Materials, (1992), 1, 85.

[19] M. Rubensteind and R.W. Ure, Jr, J. Phys. Chem. Solids, (1968), 29, 551.

[20] R. Dingle, Phys. Rev., (1969), 184, 788.